RSC Advances

PAPER

View Article Online
View Journal | View Issue

Cite this: *RSC Adv.*, 2019, **9**, 1029

Structure, tunable luminescence and energy transfer in Tb^{3+} and Eu^{3+} codoped $Ba_3InB_9O_{18}$ phosphors

Siyuan Song,[a] Jiayong Si,*[a] Jing Zhang[b] and Gemei Cai*[b]

The borate $Ba_3InB_9O_{18}$ (BIBO) is a promising host material for phosphors. A series of Tb^{3+} and Eu^{3+} codoped $Ba_3InB_9O_{18}$ phosphors were synthesized. Based on the Rietveld method, structure refinement of the codoped BIBO phosphor was carried out. Then, the luminescence properties of BIBO:Tb^{3+}, Eu^{3+} phosphors were extensively investigated under ultraviolet (UV) and vacuum ultraviolet (VUV) excitation. The measured PL spectra and decay times evidenced that energy transfer occurs between the Tb^{3+} and Eu^{3+} ions. The energy-transfer mechanism from Tb^{3+} to Eu^{3+} in $Ba_3InB_9O_{18}$ is dominated by electric multipolar interactions, with the critical distance calculated to be 10.97 Å. The temperature sensitivity of the Tb^{3+} and Eu^{3+} codoped sample under VUV was also investigated at the low temperature range from 25 K to 298 K. The emission color could be tuned from green to the red region by adjusting the concentration of codoped ions. The results indicate that the BIBO-based phosphors are valuable candidates for applications in the display and lighting fields.

Received 27th November 2018
Accepted 12th December 2018

DOI: 10.1039/c8ra09735f

rsc.li/rsc-advances

1. Introduction

Owing to their critical significance in modern lighting and display fields, such as white-light emitting diodes, vacuum fluorescent displays, cathode ray tubes, plasma display panels, X-ray imaging scintillators and field emission displays, rare earth ion-doped phosphors have attracted tremendous attention with the prevalence and boom of the electronics technology over the past few decades.[1–3] Lacking a specific color phosphor in use has prompted more investigations to be focused on full color phosphors. Fortunately, great attention has been paid to multicolor tunable luminescence due to its potential application in the fields of plasma display panels, full color displays, light emitting diodes, and field emission displays.[4,5]

Borate is regarded as a dramatic host material for phosphors because of its various crystal structures, simple process of composition, and steady physicochemistry properties.[6,7] In 2008, Cai *et al.* discovered a novel barium indium borate $Ba_3InB_9O_{18}$ (BIBO), which could be used as an X-ray detector due to its superior scintillation character.[8] The crystal structure of the BIBO compound was crystalline in the hexagonal centric structure of the $P6_3/m$ space group, which can be viewed as a layered-type structure constructed by discrete planar hexagonal $[B_3O_6]^{3-}$ rings. The $[B_3O_6]^{3-}$ rings stack parallel or antiparallel to each other along the *c*-axis. Also, layers connected with deformed BaO_6 hexagons are interleaved with regular InO_6 octahedra and BaO_9 polyhedra.[8] In the rare-earth family, Tb^{3+} is well-known as a green emitting activator due to its predominant $^5D_4$–$^7F_5$ transition peak at around 545 nm.[9] Meanwhile, the Eu^{3+} ion is considered one of the most frequently useful red emitters in rare-earth-ions-doped materials due to its $^5D_0$–$^7F_2$ transition.[10] Up to now, single Eu^{3+}- or single Tb^{3+}-doped layered-type BIBO polycrystalline structures have been investigated under UV excitation, and have shown potential applications in an illumination area due to their relatively simple preparation, intense luminescence, and large quenching concentration.[11] On the other hand, it has been recognized that the luminescence intensities of rare-earth ions can be enhanced or quenched by the energy transfer from other codoped rare-earth ions.[12,13] Moreover, Eu^{3+} and Tb^{3+} usually play the critical roles of energy transfer in displays and lightings, implying that Tb^{3+} can act as a good sensitizer to enhance the luminescence efficiency of Eu^{3+} in many host materials, such as $LiSrBO_3$, $Sr_3LaNa(PO_4)_3F$, and $Y_4Si_2O_7N_2$.[14–16] However, to the best of our knowledge, there are no reports about the photoluminescence (PL) and photoluminescence excitation (PLE) properties and the energy transfer of Tb^{3+} and Eu^{3+} in the BIBO host.

In this work, single-phase tunable green-yellow-red emitting phosphors, Tb^{3+} and Eu^{3+} codoped BIBO, were synthesized for the first time. The structure parameters and rare-earth ions occupancy were confirmed by the Rietveld refinement method. Then the luminescence properties were extensively investigated, including the photoluminescence under UV and VUV excitation, low temperature VUV spectroscopy, decay curve, and

[a]*College of Mechanical & Electrical Engineering, Central South University of Forestry & Technology, Changsha, Hunan 410004, P. R. China. E-mail: sjy98106@163.com*
[b]*School of Materials Science and Engineering, Central South University, Changsha, Hunan 410083, P. R. China. E-mail: caigemei@csu.edu.cn*

chromaticity diagram. In addition, the energy-transfer mechanism between Tb^{3+} and Eu^{3+} ions is also discussed herein.

2. Experimental section

A series of phosphors, $Ba_3In_{0.9-x}B_9O_{18}$:xTb^{3+}, $0.1Eu^{3+}$ (x = 0, 0.02, 0.05, 0.08, 0.12, 0.15, 0.18 mol) and $Ba_3In_{0.92-y}B_9O_{18}$:$0.08Tb^{3+}$, yEu^{3+} (y = 0, 0.05, 0.10, 0.15, 0.20, 0.25, 0.28 mol), were synthesized *via* standard high-temperature solid-state reaction methods. Stoichiometric mixtures of $BaCO_3$ (spectral reagent), In_2O_3 (analytical reagent), Eu_2O_3 (spectral reagent), Tb_4O_7 (spectral reagent), and H_3BO_3 (analytical reagent) were finely ground into powders in an agate mortar. The excess H_3BO_3 of 3% mol was used for compensation during the process of synthesis because of the volatilization of boron oxide at high temperature. Then, the mixtures were preheated in platinum crucibles at 650 °C for 12 h to obtain the precursors. Subsequently, the precursors underwent calcination at 980 °C for 48 h with an intermediate grinding. Finally, the obtained products were ground into homogeneous powders for the following analysis. X-ray powder diffraction data were recorded on an X-ray diffractometer (Rigaku D/Max-2500) with Cu Kα radiation and a diffracted-beam graphite monochromator operated at a power of 40 kV and 250 mA. Rietveld refinement of the structure was carried out by using the Full-Prof_suite program.[17] UV-visible diffuse reflectance (UV-DR) spectra were measured on a UV-visible spectrophotometer (Shimadzu, UV-2600) equipped with an integration sphere using $BaSO_4$ as a reference. The photoluminescence emission (PL) and excitation (PLE) spectra of Tb^{3+} and Eu^{3+} codoped BIBO under ultraviolet (UV) radiation were obtained on a Hitachi F-7000 florescence spectrophotometer equipped with a Xe lamp as the excitation source. The luminescence spectra under the vacuum ultraviolet (VUV) region were measured at Beam line 3B1B at the Beijing Synchrotron Radiation Facilities (BSRF) under normal operating conditions (220 mA). The VUV excitation spectrum was corrected by sodium salicylate since its quantum efficiency was almost constant in the region. Photoluminescence decay curves were obtained using a fluorescence spectrometer (Edinburgh, FLS-920) with a μF900 flash lamp as the excitation source. The CIE coordinates were calculated by using the PL data based on the CIE 1931 standard colorimetric system.

3. Results and discussion

3.1 Phase identification and crystal structure

The XRD patterns of the as-synthesized BIBO:xTb^{3+}, $0.1Eu^{3+}$ and BIBO:$0.08Tb^{3+}$, yEu^{3+} phosphors are shown in Fig. 1, respectively. As seen in Fig. 1a, all the patterns of the single-doped and codoped BIBO samples are consistent with the standard pattern of $Ba_3InB_9O_{18}$ (ICSD #245820) and no impurities were observed. For BIBO:xTb^{3+}, $0.1Eu^{3+}$, a pure phase of $Ba_3InB_9O_{18}$ (ICSD #245820) could be identified when Tb^{3+} varies in the range of 0–0.18 mol. Moreover, when the x value was increased, the main diffraction peaks (−120) and (014) at around 25–26° are shifted markedly toward a lower angle, indicating a lattice expansion.

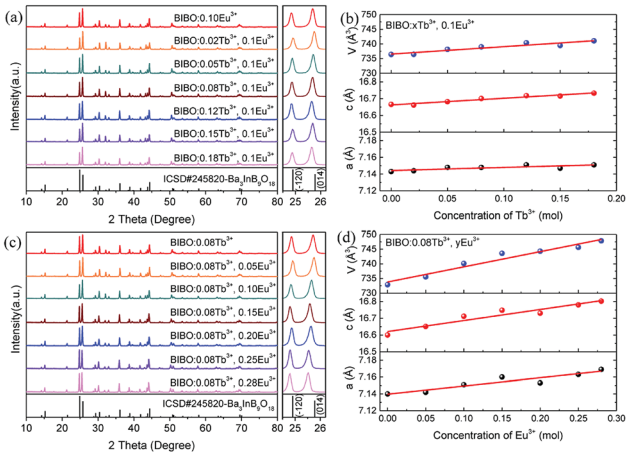

Fig. 1 (a) XRD patterns and (b) lattice parameters of BIBO:xTb^{3+}, $0.1Eu^{3+}$, (c) XRD patterns, and (d) lattice parameters of BIBO:$0.08Tb^{3+}$, yEu^{3+} samples.

This should be ascribed to the larger Tb^{3+} (r = 0.92 Å) substituting the smaller In^{3+} (r = 0.80 Å) in the $Ba_3InB_9O_{18}$ host lattice.[18] As illustrated in Fig. 1b, the measured lattice parameters, a, c, and V, increase linearly and obey Vegard's law. In addition, as shown in Fig. 1c, for BIBO:$0.08Tb^{3+}$, yEu^{3+}, no impurity phase was yet detected when the Eu^{3+} concentration was raised from 0 to 0.28 mol. As presented in Fig. 1d, by increasing the Eu^{3+} concentration, the lattice parameters of BIBO:$0.08Tb^{3+}$, yEu^{3+} also exhibit a near-linear expansion due to the substitution of smaller In^{3+} (r = 0.80 Å) by larger Eu^{3+} (r = 0.95 Å) ions.[18]

Rietveld refinement is a powerful method to investigate the crystal structure and the distribution of ions in crystal lattices. In order to understand the occupancies of the RE ions in the codoped BIBO phosphors, the structure refinement of BIBO:$0.08Tb^{3+}$, $0.25Eu^{3+}$ was performed using the Full-Prof_suite program. The crystal structure of nondoped BIBO was considered as the initial structure, with the corresponding refined pattern given in Fig. 2a. In the figure, the experimental pattern, the calculated pattern, and the difference plot are expressed by small red dots, a solid black line, and a solid blue line at the bottom, respectively. Also, the positions of the calculated Bragg reflections are marked by the vertical bars. During the refinement, a total of 43 parameters were refined, including 26 structural parameters and 17 profile parameters. The refined crystallographic parameters and reliability factors

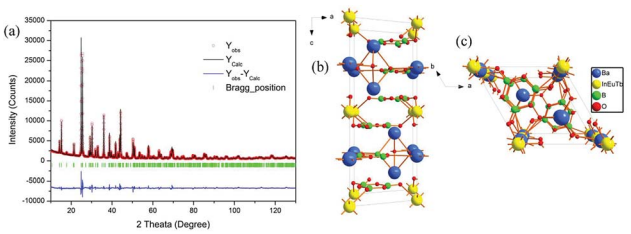

Fig. 2 (a) Rietveld refinement patterns, (b) and (c) crystal structures of the BIBO:$0.08Tb^{3+}$, $0.25Eu^{3+}$ sample.

Table 1 Experimental parameters of the powder XRD analysis and refined crystallographic data of the BIBO:0.08Tb^{3+}, 0.25Eu^{3+} sample[a]

Formula	$Ba_3In_{0.67}Tb_{0.08}Eu_{0.25}B_9O_{18}$
Diffractometer	Rigaku D/Max-2500
Radiation type	Cu Kα
Monochromator	Graphite
Wavelength (Å)	1.5405
Refined profile range 2θ (°)	10–130
Step size 2θ (°)	0.017
Step scan time per step (s)	2
Number of structure parameters	26
Number of profile parameters	17
R_B	7.38%
R_P	5.79%
R_{WP}	7.76%
S	2.60
Symmetry	Hexagonal
Space group	$P6_3/m$
a (Å)	7.1600(3)
c (Å)	16.8123(4)
Volume (Å^3)	746.43(3)
Z	2
Calculated density (g cm^{-3})	4.11

[a] $R_p = \sum|y_{io} - y_{ic}|/\sum|y_{io}|$, $R_{wp} = [\sum w_i(y_{io} - y_{ic})^2/\sum w_i y_{io}^2]^{1/2}$, $R_{exp} = [(N - P)/\sum w_i y_{io}^2]^{1/2}$.

Table 2 Atomic coordinates and isotropic displacement parameters for the BIBO:0.08Tb^{3+}, 0.25Eu^{3+} sample

Atom	Site	x	y	z	B_{iso} (Å^2)	Occ
Ba1	4f	1/3	2/3	0.13063(5)	0.247(4)	0.333(0)
In1	2b	0	0	0	0.376(8)	0.117(0)
Eu1	2b	0	0	0	0.376(8)	0.042(0)
Tb1	2b	0	0	0	0.376(8)	0.008(0)
Ba2	2a	0	0	1/4	2.41(1)	0.167(0)
O1	6h	0.454(1)	0.295(1)	1/4	−1.52(3)	1/2
O2	12i	−0.1160(9)	0.3856(9)	0.0794(3)	0.44(3)	1
O3	6h	0.596(1)	0.672(1)	1/4	0.81(4)	1/2
O4	12i	−0.0056(7)	0.7487(7)	0.0819(3)	0.55(3)	1
B1	6h	0.604(3)	0.483(3)	1/4	1.39(9)	1/2
B2	12i	−0.172(2)	0.554(2)	0.0783(6)	−0.10(4)	1

are listed in Table 1. The primary reliability factors in the structural refinement converged to R_B = 7.38%, R_P = 5.79%, R_{WP} = 7.76%, and S = 2.60, indicating that the determined structure should be reasonably accepted. The codoped BIBO:0.08Tb^{3+}, 0.25Eu^{3+} was crystallized in the space group $P6_3/m$ and in a hexagonal symmetry. The lattice parameter (a, c) and lattice volume (V) of the codoped sample were 7.1600(3) Å, 16.8123(4) Å, and 746.43(3) Å^3, respectively. The structural parameters including the atomic coordinates, atomic occupancies, and isotropic displacement are shown in Table 2. The crystal structure of $Ba_3InB_9O_{18}$:0.08Tb^{3+}, 0.25Eu^{3+} was formed by the stable stacking arrangement of B_3O_6, BaO_6, InO_6, and BaO_9 modules, with B_3O_6 layers connected by barium and indium atoms, as shown in Fig. 2b and c. The codoped Tb^{3+} and Eu^{3+} ions were demonstrated to substitute the In^{3+} sites in the host of BIBO. In addition, the Tb^{3+} and Eu^{3+} ions sites were verified by the actual experiments. We synthesized many samples with the codoped rare-earth ions occupying different cations. Using the XRD analysis and the index calculations, it was eventually found that Tb^{3+} and Eu^{3+} ions could not enter into the lattice of Ba^{2+} (r = 1.34 Å), whereas they could substitute the In^{3+} ions. This may attributed to the closed ionic radius and coordination of Eu^{3+} (r = 0.95 Å), Tb^{3+} (r = 0.92 Å), and In^{3+} (r = 0.80 Å) in the BIBO host.[18]

3.2 Photoluminescence properties

The BIBO, as a potential host for phosphors, exhibits a broad and intense emission band in the range of 360–500 nm with weak violet-blue emission on account of the recombination of an electron on a donor formed by oxygen vacancies with a hole on an acceptor consisting of indium or barium vacancies.[8,9,19] As presented in Fig. 3, the photoluminescence of single Tb^{3+}- or Eu^{3+}-doped BIBO demonstrated excellent performance for emitting intense green and red lighting when studied under UV excitation. Fig. 3a shows the excitation and emission spectra of the BIBO:0.08Tb^{3+} sample. Intense green emission at 550 nm based on the $^5D_4$–^7F_J (J = 6, 5, 4, 3) transitions of Tb^{3+} ions in BIBO host can be observed under 232 nm excitation. Under 232 nm excitation, the main excitation band is located at 232 nm due to the spin-allowed 4f^8–4f^{7}5d^1 transitions of Tb^{3+} ions.[20,21] Moreover, as seen in Fig. 3b, upon 221 nm excitation, the BIBO:Eu^{3+} phosphor exhibits a red emission, attributed to the absorption band magnetic dipole transition $^5D_0$–$^7F_1$.[22–25] The excitation spectrum was obtained by monitoring the emission of Eu^{3+} at 590 nm, and showed an absorption band ranging from 200 to 250 nm containing the excitation spectrum of Eu^{3+}. Furthermore, the broad excitation band centered at 211 nm should be assigned to the charge transfer band of $O^{2-} \rightarrow Eu^{3+}$. Fig. 3c illustrates the excitation and emission spectrum of the typical BIBO:0.08Tb^{3+}, 0.25Eu^{3+} phosphor. Once Eu^{3+} is doped into BIBO:0.08Tb^{3+}, both the Tb^{3+} green emission peak at 550 nm and the Eu^{3+} red emission at 590 nm were found in the PL spectrum of Tb^{3+}, Eu^{3+} codoped BIBO phosphor at 233 nm excitation. Monitoring the 550 nm emission, the PLE spectrum of BIBO:0.08Tb^{3+}, 0.25Eu^{3+} had a similar profile with that of BIBO:0.08Tb^{3+} and showed a peak wavelength at 233 nm, indicating effective energy transfer from Tb^{3+} ions to Eu^{3+} ions. Moreover, monitoring 590 nm emission, an obvious split in the

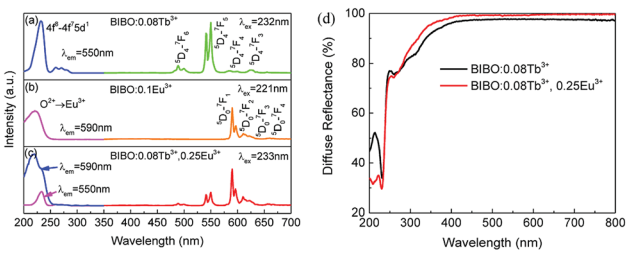

Fig. 3 UV excitation and emission spectra of (a) BIBO:0.08Tb^{3+}, (b) BIBO:0.1Eu^{3+}, and (c) BIBO:0.08Tb^{3+}, 0.25Eu^{3+}, and (d) diffuse reflectance spectra of the BIBO:0.08Tb^{3+} and BIBO:0.08Tb^{3+}, 0.25Eu^{3+} samples.

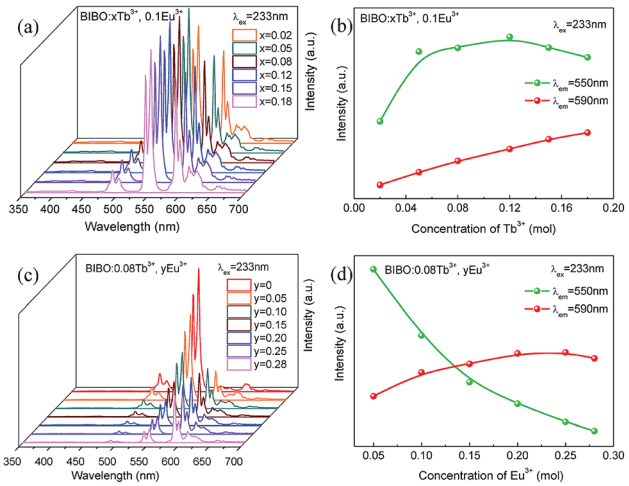

Fig. 4 (a) UV emission spectra and (b) luminescence intensity of Tb^{3+} and Eu^{3+} for BIBO:xTb^{3+}, 0.1Eu^{3+}, (c) UV emission spectra and (d) luminescence intensity of Tb^{3+} and Eu^{3+} for BIBO:0.08Tb^{3+}, yEu^{3+}.

excited band below 250 nm was found at 219 and 233 nm in the Eu^{3+} and Tb^{3+} ions codoped BIBO, corresponding to the CTB bands of Eu^{3+} and Tb^{3+} in Fig. 3a and b, implying the energy transfer from Tb^{3+} to Eu^{3+}.

In addition, the diffuse reflectance spectra of BIBO:0.08Tb^{3+} and BIBO:0.08Tb^{3+}, 0.25Eu^{3+} phosphors are given in Fig. 3d, and are consistent with the above PLE spectra. For BIBO:0.08Tb^{3+}, there were two absorption bands located in the range of 210–250 nm and 250–400 nm, respectively. The first one is attributed to both the transitions from Tb^{3+} and from the valence to conduction bands of the host lattice, meanwhile the second one is the absorption band of Tb^{3+} ions due to the transitions from the 4f to 5d states. Then for the Tb^{3+}, Eu^{3+} codoped BIBO sample, the diffuse reflectance between 210–250 nm is obviously reduced, indicating the higher absorption caused by the energy transfer of Eu^{3+} and Tb^{3+}. By the intercept method, the optical band gap was estimated as 5.34 and 5.41 eV for BIBO:0.08Tb^{3+} and BIBO:0.08Tb^{3+}, 0.25Eu^{3+}, respectively. This means that the band gap of BIBO is slightly widened by the codoped Tb^{3+} and Eu^{3+} ions.

The concentration-dependent emission spectra of BIBO:xTb^{3+}, 0.1Eu^{3+} with varying Tb^{3+} concentrations under 233 nm excitation are given in Fig. 4a and b. With increasing the Tb^{3+} concentration, the emission intensity of Eu^{3+} at 590 nm is linearly increased, whereas the red emission intensity of Tb^{3+} at 550 nm reaches the maximum at $x = 0.12$, and then generally decreases due to the concentration quenching of Eu^{3+} ions. The shapes of all PL spectra remain unchanged with varying the Tb^{3+} concentration. In addition, considering the results of single Tb^{3+}-doped BIBO phosphors, the concentration Tb^{3+} is fixed at 0.08 mol in the codoped samples.[11] Fig. 4c and d illustrate the emission spectra and luminescence intensity of Tb^{3+} and Eu^{3+} for BIBO:0.08Tb^{3+}, yEu^{3+}. With increasing the concentration of Eu^{3+}, the luminescence of Tb^{3+} decreases gradually, whereas that of Eu^{3+} first reaches a maximum at $y =$ 0.25 and then begins to decline. This further implies the energy

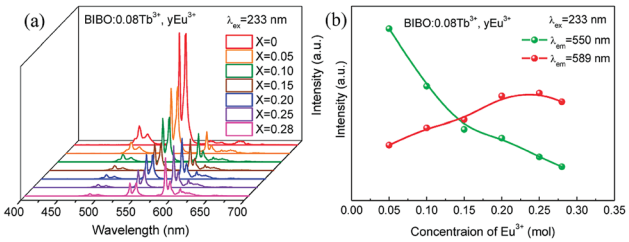

Fig. 5 (a) VUV emission spectra, and (b) luminescence intensity of Tb^{3+} and Eu^{3+} for BIBO:0.08Tb^{3+}, yEu^{3+}.

transfer from Tb^{3+} to Eu^{3+} in the BIBO host. Usually, the excitation of the isomorphic compounds of $Ba_3REB_9O_{18}$ is primarily determined by the B_3O_6 borate groups.[26–28] When ions with a smaller radius are replaced by larger ones with little electronegativity, they will attract the electrons from O^{2-} more weakly based on the bond structure of RE^{3+}–O^{2-}–B^{3+}. On this account, the electron-cloud density of the O^{2-} ion increased and it needed less energy for the electron transfer from the O^{2-} $2p^6$ valence bands to B^{3+} 2s and 2p conduction.[28] Therefore, the optimal excitation wavelength slightly increases from 232 to 233 nm, ascribed to the increasing concentration of Eu^{3+} with a larger ionic radius.

With the development of plasma display panels (PDPs) and large flat panel displays (FPDs), an economic phosphor that can be excited efficiently in the vacuum ultraviolet (VUV) range was needed to convert the VUV photons, particularly the Xe resonance emission to red, green, and blue (RGB) tricolor lights.[29,30] The synchrotron radiation light source makes investigations in the VUV region possible. Then the energy level of rare-earths in the VUV region can be acquired and assumed. The emission spectra and luminescence intensity of BIBO:0.08Tb^{3+}, yEu^{3+} under VUV excitation are presented in Fig. 5a and b. The spectra are similar to those obtained under UV conditions. Note that the red emission band of Eu^{3+} is slightly moved from 590 to 589 nm, probably due to the different excitation source compared with the Xe lamp. The intensity of emission spectra for Tb^{3+} and Eu^{3+} under the VUV region was modified as a result of Tb^{3+} and Eu^{3+} codoping into BIBO, similar to the case for the UV measurements in Fig. 4.

3.3 Energy-transfer mechanism

In order to further investigate the energy transfer from Tb^{3+} to Eu^{3+} in BIBO:Tb^{3+}, Eu^{3+} phosphors, the decay curves of the Tb^{3+} emission were measured and are illustrated in Fig. 6. Generally, a double-exponential decay behavior of an activator is frequently observed when the excitation energy is transferred from the sensitizer to activator. Hence, all decay curves of BIBO:0.08Tb^{3+}, yEu^{3+} could be well fitted using a biexponential function:[31–33]

$$I = A_1 \exp\left(-\frac{t}{\tau_1}\right) + A_2 \exp\left(-\frac{t}{\tau_2}\right) \quad (1)$$

where I is the luminescence intensity at time t, τ_1 and τ_2 refer to two components of the luminescence lifetime, A_1 and A_2 are

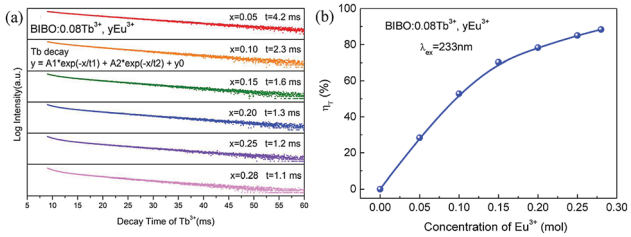

Fig. 6 (a) Decay curves for the luminescence of Tb^{3+} monitored at 550 nm, and (b) the energy-transfer efficiency for BIBO:0.08Tb^{3+}, $y$$Eu^{3+}$ phosphors.

constants, and t stands for the average decay time. According to these parameters, the average decay times (τ) can be determined by the following formula:[31–33]

$$t = \frac{A_1\tau_1^2 + A_2\tau_2^2}{A_1\tau_1 + A_2\tau_2} \quad (2)$$

The decay lifetimes of Tb^{3+} and Eu^{3+} in a series of BIBO:0.08Tb^{3+}, $y$$Eu^{3+}$ samples were obtained under the same conditions. As shown in Fig. 6a, the effective lifetime values of Tb^{3+} monitored at 550 nm were calculated as 4.2, 2.3, 1.6, 1.3, 1.2, and 1.1 ms for x = 0.05, 0.10, 0.15, 0.20, 0.25, and 0.28, respectively. In the case of energy transfer, the luminescent lifetime of a sensitizer will be shortened, because of the presence of additional decay channels that shorten the lifetime of the excited state. In this work, the decay lifetimes of Tb^{3+} descended with increasing the Eu^{3+} concentration, which demonstrated the occurrence of efficient energy transfer from Tb^{3+} to the neighboring Eu^{3+} in the BIBO host.

The energy-transfer efficiency η_T from Tb^{3+} to Eu^{3+} ions in BIBO:0.08Tb^{3+}, $y$$Eu^{3+}$ can be expressed by the formula:[34]

$$\eta_T = 1 - \frac{I_S}{I_{S0}} \quad (3)$$

where I_{S0} and I_S are the luminescence intensity of Tb^{3+} in the absence and presence of Eu^{3+}, respectively. As given in Fig. 6b, η_T was found to increase gradually with increasing the Eu^{3+} concentration, reaching a maximum of 88.4% when the concentration of Eu^{3+} was up to 0.28.

The resonant energy transfer mechanism consists of two types: exchange interaction and multipolar interaction. The critical distance between the sensitizer and activator should be shorter than 3–4 Å when the energy transfer occurs *via* the exchange interaction.[35,36] Furthermore, the critical distance of the $Tb^{3+} \rightarrow Eu^{3+}$ energy transfer R_c can be calculated *via* using the concentration quenching method, and the critical distance between Tb^{3+} and Eu^{3+} could be estimated by the following formula:[35,36]

$$R_c \approx 2\left(\frac{3V}{4\pi\chi_c N}\right)^{\frac{1}{3}} \quad (4)$$

where V stands for the volume of the unit cell, N is the number of host cations in the unit cell, and χ_c is the quenching concentration of the summation of the sensitizer of Tb^{3+} and activator of Eu^{3+}. For the BIBO host, based on V = 746.43 Å^3, N = 6, and χ_c = 0.18, the critical distance of energy transfer for Tb^{3+} and Eu^{3+} in BIBO materials was calculated to be 10.97 Å, indicating that the electric multipolar interaction dominates the energy transfer from Tb^{3+} to Eu^{3+} ions in BIBO.

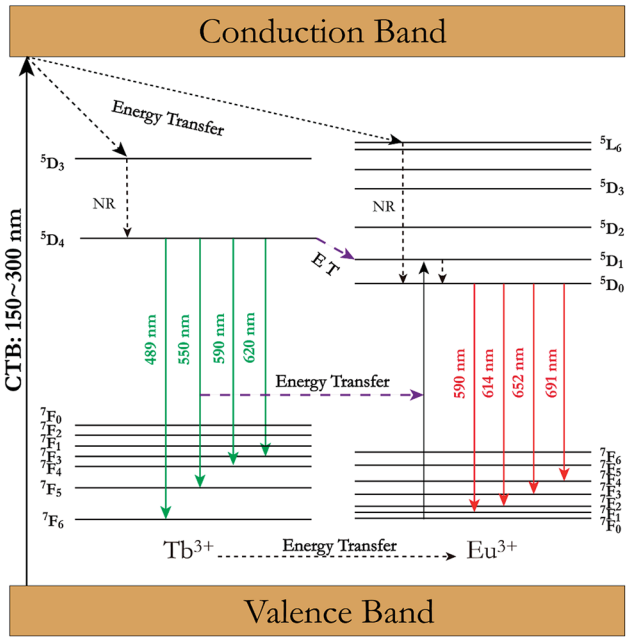

Fig. 7 Schematic energy level diagram and energy-transfer process from Tb^{3+} to Eu^{3+} in BIBO. (NR stands for nonradiative transition).

According to the above analysis, a schematic energy-level diagram and the energy transfer between Tb^{3+} and Eu^{3+} in BIBO is presented in Fig. 7. It is known that the exchange and electrostatic interaction are generated from physical interaction between the sensitizer and activator ions during the energy-transfer process. After the multistep relaxations, the excited electrons of Tb^{3+} are excited from the ground state $^7F_6$ to the excitation state $^5D_4$, and then jump to the $^7F_5$ state accompanied by energy release under 233 nm excitation. Simultaneously, the rest of the Tb^{3+} ions with the $^5D_4$ excited state transfer their energy to the $^5D_1$ excited state of Eu^{3+} ions, leading to red emission from Eu^{3+} ions through $^5D_0$–^7F_J (J = 0–6) transitions.[37–39]

3.4 Low-temperature dependence under VUV

The luminescence properties of a typical BIBO:0.08Tb^{3+}, 0.1Eu^{3+} phosphor under VUV excitation were investigated in the temperature range of 25 K and 298 K, and exhibited temperature dependence properties. As seen in Fig. 8, besides the 209 and 234 nm excitation bands, which were observed to the same to the above UV spectra, another band centered at 164 nm was demonstrated, attributed to defects in the host. Under 164 nm excitation, the wide emission band ranged from 340 to 400 nm, assigned to the intrinsic emission of the BIBO host (Fig. 8a). As shown in Fig. 8b and c, the emission spectra were also excited with 209 nm and 234 nm, which showed intensified emission at 589 and 549 nm due to the two luminescence centers of Eu^{3+} and Tb^{3+} and the energy transfer between them. The broad absorption bands of the BIBO:0.08Tb^{3+}, 0.1Eu^{3+} phosphor indicated good potential for applications in the display or

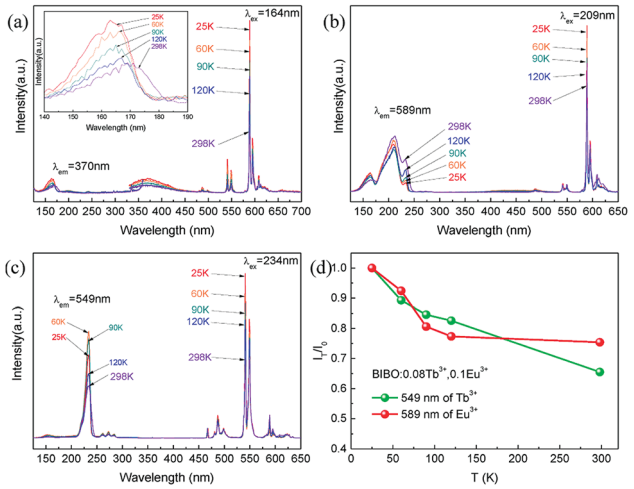

Fig. 8 The VUV excitation and emission spectra under (a) 164 nm, (b) 209 nm, (c) 234 nm excitation with different temperatures, and (d) low-temperature-dependent emission intensity of BIBO:0.08Tb^{3+}, 0.1Eu^{3+}.

lighting field. Furthermore, note that the luminescence intensity of Tb^{3+} and Eu^{3+} in the codoped BIBO phosphor was sensitive to temperature and exhibited a feature of temperature dependence (Fig. 8d). The highest emission was observed at the lowest temperature (25 K). In addition, at room temperature, the emission maximum intensity of Tb^{3+} centered at 549 nm and Eu^{3+} centered at 589 nm, respectively, declined by 34.5% and 24.6% for BIBO:0.08Tb^{3+}, 0.1Eu^{3+} as compared to the initial intensity measured at 25 K. Usually, the host lattice extension is caused by thermal expansion with the increased temperature. Then the increased bond length between the activator and the ligand leads to a decrease in the crystal field, thus reducing the transition energy.[40–42] Furthermore, the emission intensity can be fitted by using the Arrhenius equation,[43,44]

$$\frac{I_T}{I_0} = \left[1 + A \times \exp\left(-\frac{E_a}{kT}\right)\right]^{-1} \quad (5)$$

where I_0 is the initial intensity, I_T is the intensity at a given temperature T, A is a constant, k is the Boltzman constant, and E_a is the energy barrier for thermal quenching. Then the values of activation energy for thermal quenching (E_a) were calculated as 0.381 eV for Tb^{3+} and 0.469 eV for Eu^{3+}, respectively. The relatively high activation energy indicated that the emission of Eu^{3+} had a higher thermal barrier for luminescence quenching.

3.5 Tunable emissions

Under the excitation of 233 nm, the CIE chromaticity coordinates of BIBO:0.08Tb^{3+}, $y$$Eu^{3+}$ were calculated and the results are listed in Table 3. With the increasing concentration of codoped Eu^{3+} in BIBO:0.08Tb^{3+}, the emission color varied from yellowish green to orange, with the corresponding CIE chromaticity coordinates from A0 ($y = 0$) to A6 ($y = 0.28$) illustrated in Fig. 9. The results indicate that the as-obtained phosphors showed merits of multicolor emissions in the visible region when excited by a single wavelength light. The inset figures are

Table 3 CIE Chromaticity Coordinate for BIBO:0.08Tb^{3+}, $y$$Eu^{3+}$ phosphors under 233 nm excitation

No. of points	BIBO:0.08Tb^{3+}, $y$$Eu^{3+}$	CIE (x, y)
A0	$y = 0$	0.3119, 0.6127
A1	$y = 0.05$	0.3748, 0.5595
A2	$y = 0.10$	0.4203, 0.5189
A3	$y = 0.15$	0.4583, 0.4838
A4	$y = 0.20$	0.4869, 0.4586
A5	$y = 0.25$	0.5102, 0.4380
A6	$y = 0.28$	0.5194, 0.4277

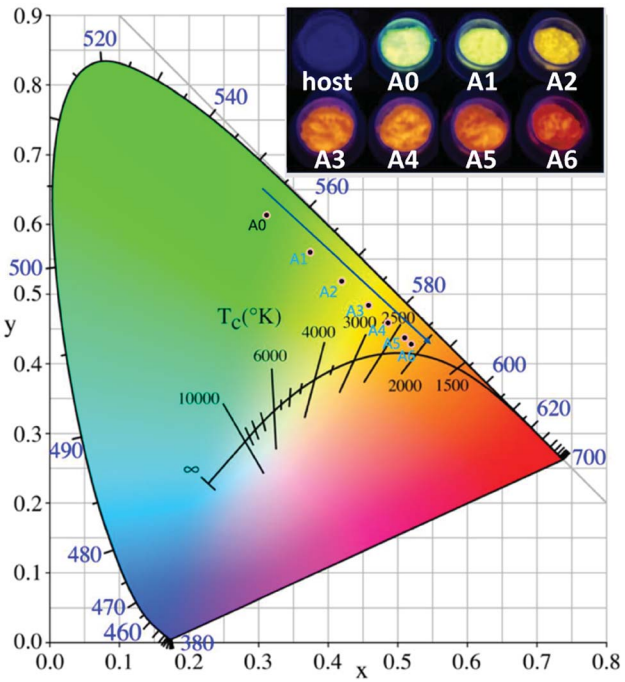

Fig. 9 CIE chromaticity diagram excited at 233 nm and the emitting color under 254 nm UV lamp excitation of BIBO:0.08Tb^{3+}, $y$$Eu^{3+}$ phosphors.

the digital photographs of BIBO:0.08Tb^{3+}, $y$$Eu^{3+}$ upon 254 nm UV-lamp excitation. As also given in the photographs of the emitting phosphors, the variation of the as-observed emitting color is obvious, which means that tunable luminescence could be realized in the novel Tb^{3+} and Eu^{3+} codoped BIBO phosphors based on effective energy transfer.

4. Conclusions

In conclusion, a series of Tb^{3+} and Eu^{3+} codoped BIBO phosphors were synthesized by high-temperature solid-state reaction. The crystal structure and the sites of Tb^{3+} and Eu^{3+} ions of BIBO:Tb^{3+}, Eu^{3+} phosphors were investigated using the Rietveld refinement method. Then the luminescence properties of BIBO:Tb^{3+}, Eu^{3+} phosphors were investigated under ultraviolet (UV) and vacuum ultraviolet (VUV) excitation. Energy transfer between Tb^{3+} and Eu^{3+} ions was demonstrated by the PL spectra and decay time. The energy-transfer mechanism from Tb^{3+} to

Eu^{3+} in $Ba_3InB_9O_{18}$ was dominated by electric multipolar interactions, with the critical distance calculated to be 10.97 Å. Moreover, the temperature sensitivity of the sample under VUV was investigated at low temperature ranging from 25 K to 298 K. The emission colors of BIBO:Tb^{3+}, Eu^{3+} could be adjusted from yellowish green to orange by tuning the content of Eu^{3+} ions under UV radiation, thus showing a great potential for their use in display and lighting fields applications.

Conflicts of interest

There are no conflicts to declare.

Acknowledgements

This work was supported by the National Natural Science Foundation of China (Grant numbers 51472273 and 51772330), and Beijing Synchrotron Radiation Facilities (BSRF). The Aid program for the Natural Science Foundation of Hunan Province (2017JJ2403), the Key Research Foundation of Education Bureau of Hunan Province (No. 16A220), and Science and Technology Innovative Research Team in Higher Educational Institutions of Hunan Province (No. 2014207) are gratefully acknowledged.

Notes and references

1 J. Zhang, G. M. Cai, L. W. Yang, Z. Y. Ma and Z. P. Jin, *Inorg. Chem.*, 2017, **56**, 12902.
2 S. P. Tiwari, A. Kumar, S. Singh and K. Kumar, *Vacuum*, 2017, **146**, 537.
3 V. V. Shinde, S. V. Shinde, N. S. Dhoble and S. J. Dhoble, *J. Inorg. Organomet. Polym.*, 2015, **25**, 593.
4 C. C. Lin, W. T. Chen, C. I. Chu, K. W. Huang, C. W. Yeh, B. M. Cheng and R. S. Liu, *Light: Sci. Appl.*, 2016, **5**, e16066.
5 C. He, Z. Xia and Q. Liu, *Opt. Mater.*, 2015, **42**, 11.
6 R. Velchuri, B. Vijaya Kumar, V. Rama Devi, G. Prasad, D. Jaya Prakash and M. Vithal, *Mater. Res. Bull.*, 2011, **46**, 1219.
7 D. Chikte, S. K. Omanwar and S. V. Moharil, *J. Lumin.*, 2013, **142**, 180.
8 G. Cai, X. L. Chen, W. Y. Wang, Y. F. Lou, J. Liu, J. T. Zhao and H. H. Chen, *J. Solid State Chem.*, 2008, **181**, 646.
9 J. S. Zhang, Z. D. Hao, X. Zhang, Y. S. Luo, X. G. Ren, X. J. Wang and J. H. Zhang, *J. Appl. Phys.*, 2009, **106**, 34915.
10 Z. J. Liang, F. W. Mo, X. G. Zhang, L. Y. Zhou, P. C. Chen and C. Y. Xu, *Ceram. Int.*, 2014, **40**, 7501.
11 G. M. Cai, F. Zheng, D. Q. Yi, Z. P. Jin and X. L. Chen, *J. Lumin.*, 2010, **130**, 910.
12 L. H. Tian, B. Y. Yu, C. H. Pyun, H. L. Park and S. I. Mho, *Solid State Commun.*, 2004, **129**, 43.
13 R. S. Kumar, V. Ponnusamy and M. S. Jose, *Eur. Phys. J.: Appl. Phys.*, 2014, **68**, 30702.
14 J. Cao, X. Li, Z. Wang, Y. Wei, L. Chen and H. Guo, *Sens. Actuators, B*, 2016, **224**, 507.
15 J. Cao, X. Wang, X. Li, Y. Wei, L. Chen and H. Guo, *J. Lumin.*, 2016, **170**, 207.
16 G. J. Wang, D. J. Pan, T. Xu, G. X. Xiang, Z. J. Zhang, H. T. Hintzen, J. T. Zhao and Y. Huang, *J. Alloys Compd.*, 2017, **708**, 154.
17 J. Rodriguez-Carvajal, *Phys. Rev. B: Condens. Matter Mater. Phys.*, 1993, **192**, 55.
18 R. D. Shannon, *Acta Crystallogr., Sect. A: Cryst. Phys., Diffr., Theor. Gen. Crystallogr.*, 1976, **32**, 751.
19 Z. X. Wang, H. Pei, X. M. Tao, G. M. Cai, R. H. Mao and Z. P. Jin, *J. Solid State Chem.*, 2018, **258**, 351.
20 M. Zawadzki, D. Hreniak, J. Wrzyszcz, W. Mista, H. Grabowska, O. L. Malta and W. Strek, *Chem. Phys.*, 2003, **291**, 275.
21 Z. Zhang, S. Zhang, W. Zhang and W. Yang, *Solid State Sci.*, 2017, **64**, 69.
22 G. Blasse and B. C. Grabmaier, *Luminescent Materials*, Springer-Verlag, Berlin, 1994.
23 S. Shionoya and W. M. Yen, *Phosphor Handbook*, CRC Press, Boca Raton, 1999.
24 S. K. Sharma and M. M. Malik, *J. Lumin.*, 2016, **173**, 231.
25 S. Jayakiruba, G. Kumar and N. Lakshminarasimhan, *Solid State Sci.*, 2016, **55**, 121.
26 G. M. Cai, M. Li, J. Liu, S. F. Jin, W. Y. Wang, F. Zheng and X. L. Chen, *Mater. Res. Bull.*, 2009, **44**, 2211.
27 G. M. Cai, M. He, X. L. Chen, W. Y. Wang, Y. F. Lou, H. H. Chen and J. T. Zhao, *Powder Diffr.*, 2007, **22**, 328.
28 C. Duan, J. Yuan, X. Yang, J. Zhao, Y. Fu, G. Zhang, Z. Qi and Z. Shi, *J. Phys. D: Appl. Phys.*, 2005, **38**, 3576.
29 B. Han, H. B. Liang, H. Y. Ni, Q. Su, G. T. Yang, J. Y. Shi and G. B. Zhang, *Opt. Express*, 2009, **17**, 7138.
30 M. B. Xie, Y. Tao, Y. Huang, H. B. Liang and Q. Su, *Inorg. Chem.*, 2010, **49**, 11317.
31 G. M. Cai, J. J. Fan, H. K. Li, Z. Zhao, L. M. Su and Z. P. Jin, *J. Alloys Compd.*, 2013, **562**, 182.
32 M. Shang, D. Geng, X. Kang, D. Yang, Y. Zhang and J. Lin, *Inorg. Chem.*, 2012, **51**, 11106.
33 T. Jiang, X. Yu, X. Xu, H. Yu, D. Zhou and J. Qiu, *Mater. Res. Bull.*, 2014, **51**, 80.
34 P. I. Paulose, G. Jose, V. Thomas, N. V. Unnikrishnan and M. K. R. Warrier, *J. Phys. Chem. Solids*, 2003, **64**, 841.
35 G. Blasse, *Philips Res. Rep.*, 1969, **24**, 131.
36 J. T. Zhang, C. Y. Ma, Z. C. Wen, M. M. Du, J. Q. Long, R. Ma, X. Y. Yuan, J. T. Li and Y. G. Cao, *Opt. Mater.*, 2016, **58**, 290.
37 Y. T. Lin, Z. R. Niu, Y. Han, C. Z. Li, W. L. Zhou, J. L. Zhang, L. P. Yu and S. X. Lian, *J. Alloys Compd.*, 2017, **690**, 267.
38 S. Loos, F. Steudel, B. Ahrens and S. Schweizer, *J. Lumin.*, 2017, **181**, 31.
39 J. Y. Si, N. Liu, S. Y. Song, G. M. Cai, N. Yang and Z. Li, *J. Alloys Compd.*, 2017, **719**, 171.
40 L. M. Su, X. Fan, G. M. Cai and Z. P. Jin, *RSC Adv.*, 2017, **7**, 22156.
41 J. S. Kim, Y. H. Park, S. M. Kim, J. C. Choi and H. L. Park, *Solid State Commun.*, 2005, **133**, 445.
42 Z. Xia, X. Wang, Y. Wang, L. Liao and X. Jing, *Inorg. Chem.*, 2011, **50**, 10134.
43 S. Bhushan and M. V. Chukichev, *J. Mater. Sci. Lett.*, 1988, **7**, 319.
44 P. Dorenbos, *J. Phys.: Condens. Matter*, 2005, **17**, 8103.